

Skill-Aware Diffusion for Generalizable Robotic Manipulation

Aoshen Huang^{*1}, Jiaming Chen^{*2}, Jiyu Cheng^{✉1}, Ran Song¹, Wei Pan², Wei Zhang¹

Abstract—Robust generalization in robotic manipulation is crucial for robots to adapt flexibly to diverse environments. Existing methods usually improve generalization by scaling data and networks, but model tasks independently and overlook skill-level information. Observing that tasks within the same skill share similar motion patterns, we propose Skill-Aware Diffusion (SADiff), which explicitly incorporates skill-level information to improve generalization. SADiff learns skill-specific representations through a skill-aware encoding module with learnable skill tokens, and conditions a skill-constrained diffusion model to generate object-centric motion flow. A skill-retrieval transformation strategy further exploits skill-specific trajectory priors to refine the mapping from 2D motion flow to executable 3D actions. Furthermore, we introduce IsaacSkill, a high-fidelity dataset containing fundamental robotic skills for comprehensive evaluation and sim-to-real transfer. Experiments in simulation and real-world settings show that SADiff achieves good performance and generalization across various manipulation tasks. Code, data, and videos are available at <https://sites.google.com/view/sa-diff>.

Index Terms—Robotic manipulation, motion planning, diffusion model, skill transfer.

I. INTRODUCTION

LANGUAGE-conditioned robotic manipulation [1], [2], [3], which involves planning executable actions according to visual observation and language instruction, has gained increasing attention. As a primary approach in this field, imitation learning has demonstrated powerful capability as it enables robots to learn directly from collected demonstrations [4], [5]. However, achieving robust generalization across various objects and environments continues to be a persistent challenge [6], as the classic imitation learning paradigm [7], [8] depends heavily on task-specific data and struggles to adapt to distributional shifts, thus affecting its adaptability and flexibility in unfamiliar scenarios.

To improve generalization in robotic manipulation, previous research has explored two main directions. One direction focuses on enhancing visual representations in the end-to-end imitation learning framework by leveraging large-scale pre-training with incorporated auxiliary objectives [9], [10], [11]. For instance, Nair et al. [10] adopted time-contrastive learning to capture robust visual patterns, while Jia et al. [11] leveraged interaction prediction to model behavioral dynamics. However, these methods typically require large-scale data and extracted visual features inevitably include task-irrelevant elements (e.g., background details or textures), reducing their efficiency and

precision. The other direction formulates imitation learning as a two-stage framework, which first learns to predict future task-relevant motion representations (e.g., task video [12], goal image [13], or scene flow [14]) from easily accessible video data, and then leverages these representations as auxiliary inputs for visuomotor policy learning or directly maps them to executable actions. Among various motion representations, flow-based approaches [15], [16] stand out for effectively emphasizing task-relevant motion dynamics while ignoring task-irrelevant visual distractions. However, attaining strong generalization with these methods remains dependent on large-scale training data. Moreover, such approaches face challenges in achieving a balance between robustness and precision when translating predicted 2D motion representations into executable 3D actions. For instance, learning-based strategies [14], [15] are sensitive to intrinsic and extrinsic camera parameters, while vanilla heuristic-based strategies [16], [17] suffer from unstable performance due to sensor noise. In contrast, this work proposes to extract and leverage the correlations across diverse tasks for data-efficient generalization rather than relying on large-scale data.

Inspired by the fact that different tasks within the same skill domain exhibit similar motion patterns [18], [19], [20], we exploit skill-level information as additional guidance and propose the Skill-Aware Diffusion (SADiff) framework to improve generalization in robotic manipulation. First, a skill-aware encoding module equips learnable skill tokens to capture skill-specific information during interacting with multimodal inputs. Then, a skill-constrained diffusion model generates object-centric motion flow conditioned on the produced skill-aware token sequences, allowing the model to capture unified features across diverse tasks within the same skill domain while preserving task-specific information. Two skill-specific auxiliary losses, i.e., skill classification and skill contrastive losses, are introduced to distinguish motion patterns across diverse skills to enhance precision and robustness. Finally, we propose a skill-retrieval transformation strategy that translates the generated 2D motion flow to executable 3D actions by retrieving skill-specific priors to refine the 2D-to-3D mapping. Through systematically incorporating skill-specific information, SADiff achieves superior generalization across diverse tasks and environments without relying on large-scale data.

Furthermore, existing robotic manipulation datasets [21], [22], [23] primarily focus on task completion rates, lacking the granularity required to evaluate specific manipulation skills. To address this limitation, we construct IsaacSkill, a new dataset specifically designed for skill-centric evaluation. Built upon the high-fidelity NVIDIA Isaac Lab platform [24], IsaacSkill covers fundamental robotic skills applied to a variety of tasks. It not only enables a comprehensive assessment of specific skill capabilities, but also provides the realistic dynamics

^{*} Contributed equally to this work. [✉] Corresponding author.

¹School of Control Science and Engineering, Shandong University, Jinan 250061, China. (email: aoshenhuang@mail.sdu.edu.cn; jycheng@sdu.edu.cn; ransong@sdu.edu.cn; info@vslab.com)

²Department of Computer Science, The University of Manchester, M13 9PL Manchester, U.K. (e-mail: ppjmchen@gmail.com; wei.pan@manchester.ac.uk)

required to support robust sim-to-real transfer.

In summary, the contributions of this work are as follows:

- 1) We propose the SADiff framework to improve generalization in robotic manipulation by explicitly modeling skill-level representations and systematically integrating them into the encoding, generation, and execution phases.
- 2) We develop a skill-constrained diffusion model that generates object-centric motion flow conditioned on skill-aware token sequences, concurrently reinforced by skill contrastive learning for robust flow generation.
- 3) We design a skill-retrieval transformation strategy that uses skill-specific priors to refine the mapping from predicted object-centric 2D motion flow to executable 3D actions, improving precision and consistency without additional training.
- 4) We construct IsaacSkill, a new dataset on the high-fidelity NVIDIA Isaac Lab platform, covering fundamental skills across diverse tasks to enable skill-centric evaluation and facilitate zero-shot sim-to-real transfer.

The rest of this article is organized as follows. Section II reviews related work. Section III presents the problem formulation. Section IV details the proposed method. Section V presents experimental results and comparisons. Section VI concludes this article.

II. RELATED WORK

In this section, we review recent works in robotic manipulation that aim at learning from demonstrations and enhancing generalization to novel tasks and environments.

A. Learning from Demonstrations in Robotic Manipulation

Imitation learning, which enables robots to directly learn from collected demonstrations, has recently become a primary approach in robotic manipulation [8], [25], [26], [27], [28], [29]. In the standard imitation learning framework, a policy network is trained to replicate expert behavior by learning a mapping from state observations to the corresponding actions [28]. For instance, ACT [8] employed a CVAE-transformer to predict k-step action chunks from visual observations, enabling effective manipulation with a few demonstrations. Chi et al. [29] proposed diffusion policy to model complex action distributions through a denoising diffusion process, efficiently handling the multimodality of trajectories in collected demonstrations.

To enhance human-robot interaction, language-conditioned imitation learning has emerged to enable robots to execute tasks following instructions, where visual inputs and language instructions are integrated to plan executable actions [1], [30], [31]. For instance, CLIPort [32] leveraged a pretrained CLIP [33] model to align visual and language features, allowing robots to directly interpret and perform language-instructed tasks. PerAct [34] employed a perceiver transformer [35] to integrate language features with voxelized RGB-D observations, enabling precise action prediction. However, these methods typically suffer from poor generalization in unseen scenarios due to their heavy reliance on extensive, task-specific demonstrations. Crucially, they often process tasks in

isolation, ignoring the shared motion patterns that cut across diverse tasks and thus struggle to adapt efficiently to new environments.

B. Improving Generalization in Imitation Learning

To enhance the generalization in imitation learning for robotic manipulation, one intuitive direction is enhancing visual encoders by pre-training on large-scale manipulation-related datasets [36], [37] in an end-to-end imitation learning framework [9], [10], [11], [38]. For instance, R3M [10] pre-trained visual encoders on human video data, using time-contrastive learning and video-language alignment to obtain robust visual features. MVP [38] leveraged masked image reconstruction to develop visual representations for generalized robotic motion control. In addition, MPI [11] introduced interaction prediction as an auxiliary objective to model behavioral patterns and physical interactions, improving the generalization of the visuomotor policy. However, these methods typically rely on large-scale datasets for pre-training, which requires labor-intensive demonstration collection and massive computational resources. More importantly, extracted visual representations often contain task-irrelevant details, such as background clutter and textures, which inevitably affect performance.

Another key direction formulates imitation learning as a two-stage framework [12], [14], [39]. The first stage focuses on predicting future task-relevant motion representations, such as task video [12], goal image [13], and scene flow [14]. In the second stage, these representations are used as auxiliary inputs to facilitate visuomotor policy learning or directly transformed into executable actions. Among diverse motion representations, motion flow in 2D pixel space has become a powerful intermediate representation in motion planning since it can be easily extracted from raw video data with advancing point tracking methods and learned at scale [39]. Representative, Track2Act [14] employed a goal-conditioned grid flow model to generate future trajectories for query points and translated these trajectories into residual actions via a policy network. Im2Flow2Act [15] learned object-centric motion flow to capture the dynamics of the target objects and translated the motion flow into actions via a flow-conditioned policy network, facilitating embodiment-agnostic manipulation. However, these methods still rely heavily on large-scale datasets. In general, previous methods tend to treat tasks in isolation, thereby overlooking shared prior across diverse tasks and ignoring the explicit modeling of skill-level information. As a consequence, such methods often struggle to effectively transfer knowledge to unseen scenarios. In contrast, we explicitly incorporate skill-specific representations to bridge different tasks, thereby enhancing generalization to new scenarios with similar underlying mechanics.

C. Diffusion Model in Robotic Manipulation

Recently, the diffusion model has shown remarkable potential in robotic manipulation [40], [41], [42]. By iteratively denoising noise into structured actions or trajectories,

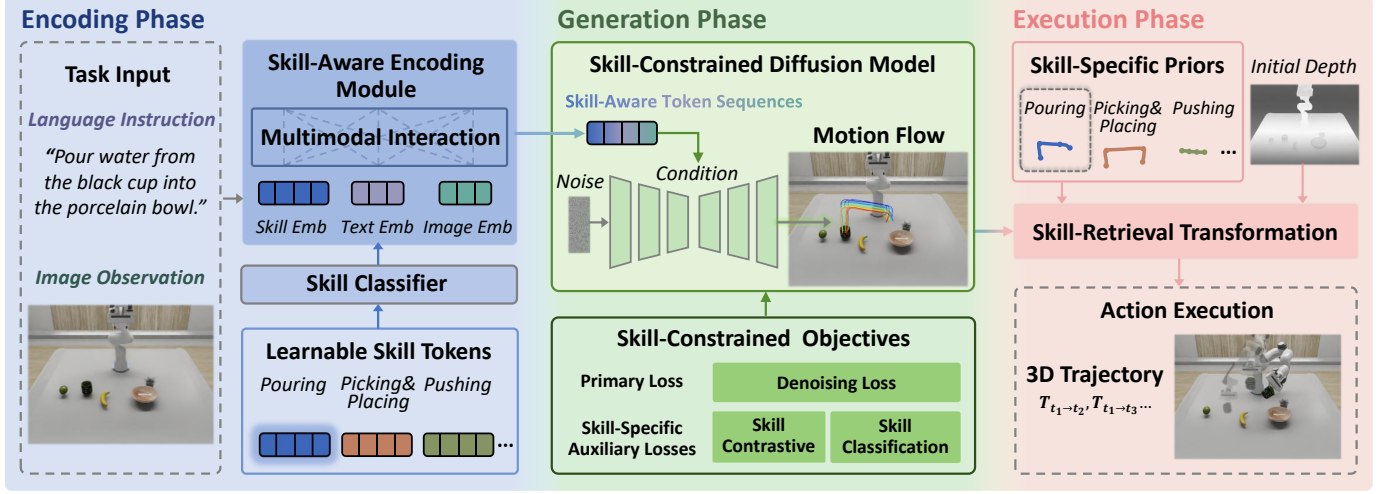


Fig. 1. Overview of the proposed Skill-Aware Diffusion (SADiff) framework. It is structured into three phases: (1) The encoding phase, where the skill-aware encoding module uses learnable skill tokens to interact with multimodal inputs and extract skill-specific information; (2) The generation phase, in which a skill-constrained diffusion model generates object-centric motion flow conditioned on the skill-aware token sequences, optimized by both denoising loss and two skill-specific auxiliary losses; and (3) The execution phase, which employs a skill-retrieval transformation strategy to translate the generated 2D motion flow into executable 3D trajectories by leveraging skill-specific priors.

diffusion-based approaches can effectively model the variability in demonstrations, enabling smooth action generation [43]. Previous works have pioneered the integration of denoising diffusion probabilistic models (DDPMs) into visuomotor control, achieving superior performance by modeling the conditional probability of actions given visual inputs [29], [44]. Subsequent research has further refined this paradigm by incorporating richer multimodal information (e.g., 3D visual representations [45] and tactile feedback [46]) together with more expressive geometric and semantic conditioning mechanisms [47], thereby improving spatial reasoning and controllability of visuomotor policies.

Some methods [17], [48], [49] leveraged diffusion models to generate future videos that serve as guidance for manipulation. For instance, UniPi [49] employed a language-conditioned video diffusion model to synthesize future frames, subsequently using an inverse dynamics model to infer actions for execution. Unlike video-based methods that capture environmental details, flow-based methods focus on task-relevant motion dynamics, enabling more direct modeling of action-related movement patterns [14], [15], [50]. Following Im2Flow2Act [15], SADiff adopts object-centric flow as the intermediate motion representation of task dynamics. Benefiting from the systematic integration of skill information into both the flow generation process and the 2D-to-3D action transformation, SADiff achieves improved robustness and generalization in various scenarios.

III. PRELIMINARIES

A. Problem Formulation

Following existing works such as Im2Flow2Act [15] and Track2Act [14], we decompose the robotic manipulation problem into two sub-problems. The first is flow generation, which aims to interpret the task from image observation and language instruction, and produce dense 2D motion flow that describes

the pixel-level movement of the target object over a time horizon. The second sub-problem is to lift the 2D motion flow into a 3D trajectory and convert it into a sequence of executable actions through a flow transformation stage.

Formally, given the task input of initial image observation I and language instruction L , the first sub-problem is to learn a flow generator \mathcal{G} that maps them to a 2D motion flow F :

$$F = \mathcal{G}(I, L) \quad (1)$$

where $F = \{P_1, P_2, \dots, P_T\}$ represents the pixel-wise motion of the target object across T time steps, P_t denotes a set of the 2D coordinates of keypoints on the target object at time step t . The second sub-problem is to design a transformation strategy \mathcal{T} that maps the predicted flow F to an executable action sequence A :

$$A = \mathcal{T}(F) \quad (2)$$

where $A = \{a_1, a_2, \dots, a_T\}$ denotes the action sequence of end-effector over the task horizon, where each action a_t represents the 6-DoF end-effector pose at time step t . We detailed the proposed approach in the following section.

B. Motion Flow Extraction

We adopt the similar paradigm of motion flow extraction as Im2Flow2Act [15]. First, we employ Qwen-VL [51] as an open-set detector to identify and locate the target object in the first frame of the video demonstration and obtain the corresponding bounding box. Then we uniformly sample a set of key points $P_1 \in \mathbb{R}^{2 \times N_x \times N_y}$ within the bounding box, where the first channel represents the 2D coordinates of the points, and $N_x \times N_y$ indicates the number of sampled points. Next, we employ TAPIR [52] as a key-point tracker, which tracks the motion of each key-point across the entire video demonstration, yielding the motion flow of the target object. The extracted motion flow can be denoted

as $F = \{P_1, P_2, \dots, P_T\} \in \mathbb{R}^{2 \times N_x \times N_y \times T}$, where each P_t corresponds to the tracked key points in frame t , and T is the total number of frames in the demonstration. The extracted motion flow serves as the training sample for the diffusion model.

IV. METHOD

Fig. 1 presents the overview of SADiff. Its key components are detailed as follows: Section IV-A introduces the skill-aware encoding module, which employs a set of learnable skill-aware tokens to capture skill-specific information while interacting with multimodal task inputs. Section IV-B introduces the skill-constrained diffusion model that generates the motion flow of the target object conditioned on the skill-aware token sequences. We design a multi-objective training paradigm for flow generation that particularly introduces a skill contrastive training method for enhancing robustness. Finally, Section IV-C details the skill-retrieval transformation strategy, which uses skill-specific trajectory priors to guide the optimization-based transformation process, accurately converting the 2D motion flow into executable 3D actions.

A. Skill-Aware Encoding

We design a skill-aware encoding module that performs interaction between multimodal inputs and extracts skill-specific information, as illustrated in Fig. 2. The encoding process begins with an RGB image captured by a camera, represented as $I \in \mathbb{R}^{H \times W \times 3}$. Given a language instruction L , such as “Pour water from the black cup into the porcelain bowl”, we use an advanced vision-language model, i.e., Qwen-VL [51], to identify and locate target objects “black cup” and “porcelain bowl”, extracting their bounding boxes $B \in \mathbb{R}^{N_o \times 4}$, where N_o represents the number of related objects. To capture skill-specific information and facilitate dynamic interactions across multimodal inputs, we introduce a set of learnable skill tokens, which are randomly initialized and represented as $S \in \mathbb{R}^{N_s \times D}$, where N_s denotes the number of skills. For a given task, skill-relevant tokens $S_i \in \mathbb{R}^D$, are selected from S based on image observation I and language instruction L with an MLP-based skill classifier, where i is the index of the relevant skill. Furthermore, we encode I , L , B , and S_i independently to obtain initial token sequences v_I , v_L , v_B , v_{S_i} , all transformed to a common encoding dimension D . Specifically, we use the pre-trained CLIP [33] to encode both image and language. The bounding boxes are encoded using 2D sinusoidal positional encoding [53], capturing spatial relationships. And the skill tokens are encoded using a simple fully-connected layer.

To generate semantically rich skill representations and enable effective information exchange across multimodal token sequences, we employ multi-head self-attention (MHSA) and multi-head cross-attention (MHCA) [54]. These mechanisms enhance the interaction of image, text, and bounding box tokens with skill tokens, facilitating the alignment and fusion of multimodal information. For conciseness, the MHSA and MHCA mechanisms are formally defined as follows:

$$\text{MHSA}(X) = \sigma(f_Q(X)f_K(X)^\top)f_V(X) \quad (3)$$

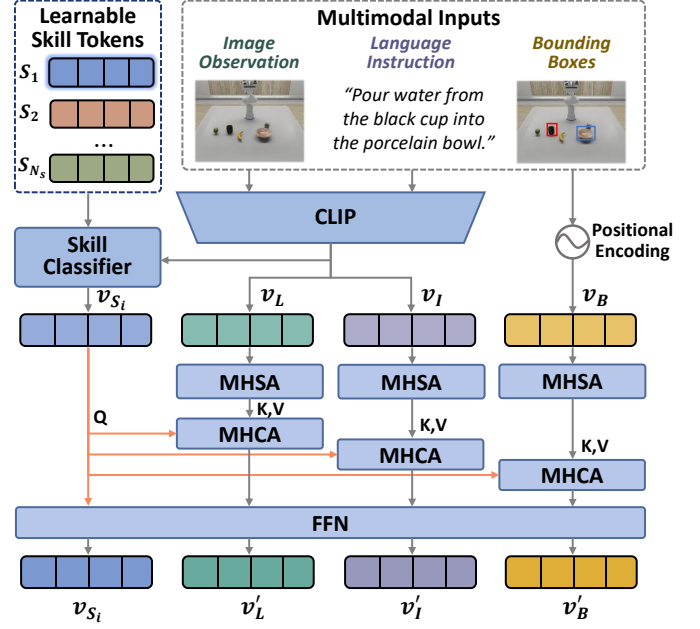


Fig. 2. Architecture of the skill-aware encoding module. The skill-aware encoding module integrates image, language, and bounding boxes of relevant objects with learnable skill tokens through attention-based interactions, producing skill-aware token sequences.

and

$$\text{MHCA}(X, Y) = \sigma(f_Q(X)f_K(Y)^\top)f_V(Y) \quad (4)$$

where σ is the softmax function, while f_Q , f_K , and f_V represent the query, key, and value mapping functions, respectively.

The multimodal token sequences v_I , v_L , v_B first undergoes initial self-encoding via MHSA, then the skill token sequences act as the query inputs, while the remaining token sequences serve as key and value inputs in MHCA. This process is followed by a feed-forward network (FFN) implemented with multi-layer perceptrons (MLPs). The interaction process is expressed as:

$$v'_x = \text{FFN}(\text{MHCA}(v_{S_i}, \text{MHSA}(v_x))) \quad (5)$$

where $x \in \{I, L, B\}$. The resulting skill-aware token sequences $v_{S_i}, v'_I, v'_L, v'_B$ are used as conditioning inputs for the diffusion model in the subsequent flow generation stage. Unlike existing methods [15] that often process multimodal inputs independently and rely on static feature alignment, our skill-aware encoding module introduces learnable skill tokens and leverages MHSA and MHCA mechanisms to dynamically align and fuse skill-specific features across modalities. Through this encoding process, the resulting skill-aware token sequences capture shared features across diverse tasks within the same skill category, while preserving task-specific details, thereby providing an effective condition for the following skill-constrained diffusion model.

B. Skill-Constrained Flow Generation

To generate a precise 2D object motion flow that is aligned with a specific skill, the current task, and the target objects, we propose a novel skill-constrained diffusion model. This model

is equipped with a denoising loss to supervise flow generation and two auxiliary skill-specific losses that guide the model to capture semantic clues related to the skill. We first introduce the diffusion model for flow generation, and then explain how we design and leverage denoising loss and two auxiliary losses to train the model.

1) *Diffusion Model for Flow Generation*: First, the motion flow F is encoded into a latent representation space using a pre-trained VAE [55] encoder $E_\phi(\cdot)$, denoted as:

$$z_0 = E_\phi(F) \quad (6)$$

where z_0 is the initial latent representation of the flow. Then the latent representation z_0 is perturbed over k steps using the forward diffusion process to derive the perturbed latent representation z_k :

$$z_k = \sqrt{\bar{\alpha}_k} z_0 + \sqrt{1 - \bar{\alpha}_k} \epsilon, \epsilon \sim \mathcal{N}(0, I) \quad (7)$$

where $\bar{\alpha}_k$ is the cumulative noise schedule at step k and $\mathcal{N}(0, I)$ is Gaussian noise distribution.

Subsequently, z_k is processed by a UNet-based noise prediction network ϵ_θ to predict perturbed noise, conditioned on skill-aware token sequences $\mathbf{v}_{S_i} = [v_{S_i}, v'_I, v'_L, v'_B]$:

$$\hat{\epsilon} = \epsilon_\theta(z_k, \mathbf{v}_{S_i}) \quad (8)$$

where $[\cdot]$ is the concatenation operation, and $\hat{\epsilon}$ is the predicted noise. Aligning with AnimatedDiff [56] and Im2Flow2Act [15], we integrate an MHSA layer as a motion module into ϵ_θ that performs information exchange on each spatial feature along the temporal dimension to capture temporal dependencies across frames.

During inference, the reverse diffusion process starts by sampling random noise $\hat{z}_m \sim \mathcal{N}(0, I)$ in the latent space. Then we iteratively denoise m times to generate the latent \hat{z}_0 . Finally, a pre-trained decoder $D_\phi(\cdot)$ maps the latent \hat{z}_0 back to the pixel-space to generate object motion flow \hat{F} :

$$\hat{F} = D_\phi(\hat{z}_0). \quad (9)$$

2) *Skill-Constrained Training*: To ensure that the generated motion flow is precise and aligned with the intended skill, we train the diffusion model with a combination of the primary denoising loss for flow generation and two skill-specific auxiliary losses. Fig. 3 illustrates the overview of the skill-constrained diffusion model and its optimization objectives.

Denoising Loss: Consistent with previous diffusion-based approaches [15], [56], [57], we adopt a mean squared error (MSE) loss between the predicted noise $\hat{\epsilon}$ and the ground-truth noise ϵ :

$$\mathcal{L}_{\text{MSE}} = \|\hat{\epsilon} - \epsilon\|^2. \quad (10)$$

This objective facilitates precise denoising by minimizing the divergence between predicted and ground-truth noise.

Skill Classification Loss: To enable the skill-aware encoding module to select the optimal skill-relevant tokens from the full set of learnable skill tokens $S \in \mathbb{R}^{N_s \times D}$, we design an auxiliary classification branch based on MLPs. Specifically, the image feature v_I and the language feature v_L encoded by the pre-trained CLIP encoder are concatenated and passed through the MLP-based skill classifier to predict

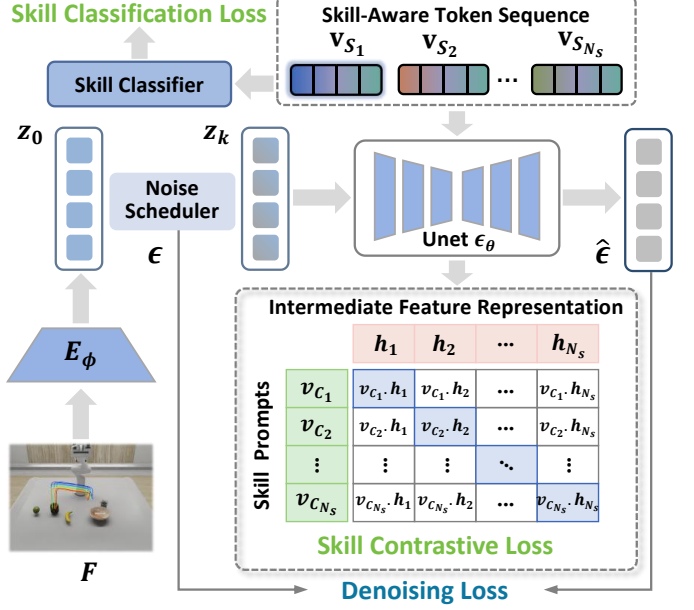


Fig. 3. Overview of the skill-constrained diffusion model. The diffusion model generates motion flow by jointly optimizing skill classification loss, skill contrastive loss, and denoising loss to ensure accurate skill selection, semantic alignment, and precise flow generation.

the skill category \hat{y}_i , which indicates the most relevant skill tokens $S_i \in \mathbb{R}^D$. The selected tokens S_i are then used in the subsequent multimodal encoding stage as described in Section IV-A, ensuring that the skill-aware token sequences are produced correctly. To supervise this skill classification, we adopt a standard cross-entropy (CE) loss:

$$\mathcal{L}_{\text{CE}} = - \sum_{i=1}^{N_s} y_i \log(\hat{y}_i) \quad (11)$$

where y_i represents the one-hot encoded ground truth label for the skill category and \hat{y}_i denotes the predicted logits.

Skill Contrastive Loss: To further ensure that the diffusion model distinguishes between motion patterns of different skills and aligns them with their semantic descriptions, we propose a skill contrastive loss that aligns the intermediate features of ϵ_θ with the semantic representations of the pre-defined skill prompts. Specifically, we construct a skill prompt bank $\mathbf{v}_C \in \mathbb{R}^{N_s \times D}$ by encoding high-level skill categories (e.g., “Pouring”, “Picking and Placing”) using the CLIP text encoder. For the target skill token S_i , the skill-aware token sequences are computed according to Eq. (5), yielding the positive skill-aware sequence $\mathbf{v}_{S_i} = [v_{S_i}, v'_I, v'_L, v'_B]$, which is then feed as the condition for the UNet ϵ_θ . We then extract the hidden feature representation from the middle layer of the UNet and project it to match the dimensionality of the CLIP features, which produces h_i .

To construct negative pairs, we treat all other skill tokens $S_j \in \mathbb{R}^D$ ($j \neq i$) as negative instances which are processed identically to the positive sample to generate mismatching intermediate features h_j . Consequently, the positive pair (h_i, v_{C_i}) is contrasted against the negative pairs (h_j, v_{C_i}) to

enforce semantic alignment in the feature space. We utilize cosine similarity to quantify the alignment:

$$\alpha_{i,j} = \cos(h_i, v_{C_j}) \quad (12)$$

The skill contrastive loss is formulated as:

$$\mathcal{L}_{\text{Contrastive}} = -\log \frac{\exp(\alpha_{i,i}/\tau)}{\exp(\alpha_{i,i}/\tau) + \sum_{j \neq i} \exp(\alpha_{i,j}/\tau)} \quad (13)$$

where τ is a temperature parameter. This objective encourages the model to align the intermediate feature h_i of the correct skill token with its corresponding skill prompt v_{C_i} , while pushing the features h_j derived from incorrect skill tokens away from that prompt. This skill contrastive loss effectively constrains the diffusion model to distinguish between motion patterns of different skills during the denoising process.

Overall Objective: The overall training objective is the weighted combination of the denoising loss and the two skill-constrained objectives:

$$\mathcal{L}_{\text{total}} = \mathcal{L}_{\text{MSE}} + \omega_1 \mathcal{L}_{\text{CE}} + \omega_2 \mathcal{L}_{\text{Contrastive}} \quad (14)$$

where ω_1 and ω_2 are hyperparameters that balance contributions of respective loss. By jointly optimizing these losses, the model learns to predict motion flow that is spatially precise and semantically aligned with the intended skill, thereby achieving robust and skill-aware motion flow generation.

C. Skill-Retrieval Transformation from Flow to Actions

Mapping the predicted object-centric 2D motion flow $\hat{F} = \{P_1, P_2, \dots, P_T\}$ into 3D space and transform it into executable actions is a critical step. In this section, we first formulate the conventional geometric optimization approach typically used, which serves as the foundation for our method. Subsequently, we will introduce our skill-retrieval strategy designed to refine this process.

1) *Motion Estimation via Geometric Optimization:* Given the initial depth observation captured by the RGB-D camera, the key-point set P_1 in the first frame of \hat{F} is back-projected into 3D space, resulting in $\mathcal{P}_1 \in \mathbb{R}^{N \times 3}$, where N represents the total number of tracked points. To obtain the 3D trajectory of the task-related object, we follow the standard formulation in AVDC [17], modeling the rigid motion from the initial frame t_1 to any subsequent frame t using a transformation matrix $\mathbf{T}_{t_1 \rightarrow t} \in \mathbb{R}^{4 \times 4}$. This matrix consists of a rotational component $\mathbf{R}_{t_1 \rightarrow t}$ and a translational component $\mathbf{t}_{t_1 \rightarrow t}$, describing the object's change in position and orientation within the camera coordinate system. To estimate $\mathbf{T}_{t_1 \rightarrow t}$ corresponding to the predicted 2D motion flow \hat{F} , we initialize it as an identity matrix and optimize the parameters by minimizing the reprojection error:

$$E_t = \sum_{n=1}^N \|P_{t,n} - K\mathbf{T}_{t_1 \rightarrow t}\mathcal{P}_{1,n}\|^2 \quad (15)$$

where E_t denotes the optimization objective, $P_{t,n}$ is the n -th point in frame t of the predicted flow, K denotes the camera intrinsic matrix, and $\mathcal{P}_{1,n}$ represents the 3D coordinates of the n -th point in \mathcal{P}_1 . By minimizing E_t using a non-linear least squares algorithm, such as Levenberg–Marquardt [58], we can obtain the optimized transformation matrix $\hat{\mathbf{T}}_{t_1 \rightarrow t}$.

Algorithm 1: Skill-Retrieval Transformation Strategy

Input : Predicted 2D motion flow $\hat{F} = \{P_1, \dots, P_T\}$, initial depth frame, camera intrinsics K , skill templates ψ , skill category s
Output: Optimized 3D transformations matrix $\{\hat{\mathbf{T}}_{t_1 \rightarrow t}\}_{t=1}^T$

- 1: Back-project keypoints P_1 using initial depth to obtain initial 3D points $\mathcal{P}_1 \in \mathbb{R}^{N \times 3}$;
- 2: Retrieve skill template $\psi_s \in \mathbb{R}^{T \times 3}$ corresponding to skill category s ;
- 3: Align $\psi_s \in \mathbb{R}^{T \times 3}$ with initial object configuration to obtain trajectory prior $\varphi \in \mathbb{R}^{T \times 3}$;
- 4: **for** $t = 1$ **to** T **do**
- 5: Initialize transformation $\mathbf{T}_{t_1 \rightarrow t} \leftarrow \mathbf{I}_{4 \times 4}$;
- 6: Define joint optimization objective E_t by Eq. (16);
- 7: Optimize E_t using a non-linear least squares algorithm (e.g., Levenberg–Marquardt) to obtain $\hat{\mathbf{T}}_{t_1 \rightarrow t}$;
- 8: **return** $\{\hat{\mathbf{T}}_{t_1 \rightarrow t}\}_{t=1}^T$

2) *Skill-Retrieval Transformation Strategy:* While minimizing reprojection error theoretically allows for the mapping of predicted 2D motion flow to 3D trajectories, practical deployments are often hindered by depth ambiguities in subsequent frames and sensor noise, which can lead to trajectory inaccuracies and discontinuities. To address these limitations, we introduce skill-specific trajectory priors into the optimization framework. These priors act as high-level guides, constraining the optimization process to motion patterns that are consistent with the intended skill, thereby enhancing both precision and physical consistency.

Specifically, we first construct a bank of trajectory templates offline. Utilizing monocular depth estimation (e.g., DepthAnythingV2 [59]), we obtain pseudo-depth maps from video demonstrations to lift the extracted 2D motion flows into 3D space. For each skill category, we compute the average 3D trajectory from relevant demonstrations and normalize it spatially. The resulting normalized trajectories form a set of templates $\psi \in \mathbb{R}^{N_s \times T \times 3}$, where N_s denotes the number of skills and T represents the temporal sequence length. During the deployment phase, we retrieve the template $\psi_i \in \mathbb{R}^{T \times 3}$ corresponding to the predicted skill category of the current task. This normalized template is spatially aligned through translation and scaling based on the initial configuration of the task-related object, yielding a task-specific trajectory prior denoted as $\varphi \in \mathbb{R}^{T \times 3}$.

We introduce this prior into the optimization process by refining the objective function defined in Eq. (15). The modified objective encourages the estimated 3D trajectory to minimize geometric reprojection error while simultaneously aligning with the retrieved skill prior:

$$E_t = \sum_{n=1}^N \|P_{t,n} - K\mathbf{T}_{t_1 \rightarrow t}\mathcal{P}_{1,n}\|^2 + \lambda \sum_{n=1}^N \|\mathcal{P}_{t,n} - \varphi_t\|^2 \quad (16)$$

where $\mathcal{P}_{t,n} = \mathbf{T}_{t_1 \rightarrow t}\mathcal{P}_{1,n}$ represents the transformed 3D

| IsaacSkill Dataset | | | | | |
|--------------------|--|--|--|--|--|
| Skills | Pouring | Picking&Placing | Pushing | Slide Opening | Hinge Opening |
| Scenes | | | | | |
| Tasks | <p>Pour water from the {black cup, yellow cup, red can} into the {porcelain bowl, red bowl, pan}.</p> | <p>Put the {lemon, rubik's cube, chess} on the {porcelain plate, white tray, chessboard}.</p> | <p>Push the {blue jar, purple cube, wooden block} to the side of {cutting board, orange tray, black photo}.</p> | <p>Open the {top, middle, bottom} layer of the {brown, red, yellow} drawer.</p> | <p>Open the {brown, white, yellow} cabinet.</p> |

Fig. 4. Overview of the constructed IsaacSkill dataset. The dataset comprises five fundamental manipulation skills: “Pouring”, “Picking&Placing”, “Pushing”, “Slide Opening”, and “Hinge Opening”. Each skill includes three different tasks involving different objects.

coordinate in frame t , φ_t denotes the corresponding waypoint from the skill prior φ , and λ is a hyperparameter balancing the two terms. By optimizing this joint objective, the system produces a transformation matrix $\hat{T}_{t_1 \rightarrow t}$ that are not only geometrically plausible but also robust to noise and faithful to the characteristic motion patterns of the skill. The complete pipeline of skill-retrieval transformation strategy is summarized in Algorithm 1.

3) *Mapping to Executable Actions*: The optimized transformation matrix is further transformed from the camera coordinate system to the robot base coordinate system. By applying the relative offset between the end-effector and the object, we derive the target 3D end-effector path. Inverse Kinematics (IK) is then applied to generate smooth joint position and velocity commands, completing the mapping from 2D flow to executable robotic actions.

V. EXPERIMENTS

In this section, we first introduce the dataset construction in Section V-A, followed by the training details in Section V-B. Section V-C presents comparative evaluations across within-distribution, challenging generalization, and skill adaptation settings, alongside component-wise ablation studies in simulation. Section V-D verifies the method’s generalization and zero-shot sim-to-real transfer capabilities in real-world scenarios. Finally, Section V-E evaluates the scalability and compositability of the proposed approach.

A. Dataset Construction

While datasets such as Meta-World [21], RLBench [22], and LIBERO [23] have advanced the field of robotic manipulation, they rely on simplistic simulations with coarse physics and limited visual fidelity. Crucially, these simplified environments fail to capture the complex dynamics required for real-world interaction, rendering them inadequate for rigorous generalization evaluation and zero-shot sim-to-real transfer. To bridge this fidelity gap, we constructed IsaacSkill, a novel dataset built on the high-fidelity NVIDIA Isaac Lab [24] platform,

ensuring physically accurate dynamics and photorealistic scenarios. Furthermore, unlike prior works [15], [14], [17] that focus on a narrow set of isolated tasks, IsaacSkill is structured around 5 fundamental robotic skills: “Pouring”, “Picking & Placing”, “Pushing”, “Slide Opening”, and “Hinge Opening”. This skill-centric approach allows us to encompass a wide variety of tasks involving diverse objects and scenarios, as shown in Fig. 4. To ensure robustness, we design 3 different tasks per skill, introducing high variability in object geometry, texture, and placement, alongside randomized distractor objects. In total, the dataset comprises 2,400 trajectory demonstrations (160 per task), providing a comprehensive benchmark for skill-generalizable manipulation.

In our dataset, the robotic platform consists of a Franka Emika Panda manipulator equipped with a parallel-jaw gripper. A single RGB camera is mounted in a third-person perspective, positioned at an elevated frontal angle to capture the entire workspace. During data collection, we employ an oracle policy to ensure successful execution for each task. The resulting demonstrations are recorded as single-view RGB videos and temporally downsampled to 32 frames to maintain consistency. To extract the motion flow of task-relevant objects, we leverage Qwen-VL [51] to first localize target objects based on language instructions. Subsequently, keypoints are uniformly sampled within the detected bounding boxes and tracked throughout the video sequence using the TAPIR tracker [52].

B. Training Details

The training process is decoupled into two stages. In the first stage, the encoder $E_\phi(\cdot)$ and the decoder $D_\phi(\cdot)$ are trained within an autoencoder framework. We initialize both components using pre-trained Stable Diffusion [60] weights, but keep the encoder frozen while fine-tuning the decoder on our dataset. In the second stage, the noise prediction network ϵ_θ is trained. Its parameters are also initialized from Stable Diffusion [60], except for the motion module, which is trained from scratch. The remaining layers are fine-tuned using Low-

Rank Adaptation [61] (LoRA) to ensure parameter efficiency. We employ the AdamW optimizer with an initial learning rate of 1×10^{-5} , utilizing a cosine decay schedule. The hyperparameters for the loss function in Eq. (14) are set to $\omega_1 = 0.01$ and $\omega_2 = 0.02$. All training is conducted on four NVIDIA A100 GPUs.

C. Simulation Experiments

1) *Experiment Setup*: We conduct simulation experiments on the proposed IsaacSkill dataset. Four baseline methods representing diverse paradigms are selected for comparison:

- *R3M* [10]: A behavior cloning approach utilizing pre-trained visual representations. It leverages temporal contrastive learning and video-language alignment to extract semantically rich features for robust policy learning.
- *AVDC* [17]: A video prediction framework that synthesizes task-specific future frames and derives executable actions by analyzing dense pixel correspondences between adjacent predicted frames.
- *Track2Act* [14]: A trajectory-centric method that employs a goal-conditioned grid flow model to generate future trajectories for query points. These trajectories are subsequently mapped to residual actions via a specific policy network.
- *Im2Flow2Act* [15]: A flow-based approach that generates object-centric motion flows, which serve as conditions for a policy network to output executable actions.

To comprehensively evaluate the effectiveness and robustness of the proposed SADiff, we structure our simulation experiments into four main parts:

- *Within-Distribution Comparative Experiment*: We first assess the fundamental imitation capabilities of SADiff and baselines on tasks consistent with the training distribution.
- *Robustness and Generalization Analysis*: We rigorously test the model's robustness against variations in visual context, object instances, categories, and robotic embodiments to evaluate out-of-distribution performance.
- *Instruction-Guided Skill Adaptation Experiment*: We examine the model's flexibility in adapting to changing language instructions while the scene configuration remains constant.
- *Ablation Studies*: Finally, we isolate and quantify the contributions of key components, including learnable skill tokens, skill contrastive loss, and skill-specific trajectory priors.

In all the aforementioned experiments, we compare our method against baselines over 25 independent rollouts, reporting the average Success Rate (SR) as the primary metric. To ensure robust evaluation, each rollout features randomly initialized positions for task-related objects, as well as randomized types and placements for interfering objects. In the following sections, we present the detailed results and analysis for each experimental setting.

2) *Within-Distribution Comparative Experiment*: To evaluate the fundamental imitation capability of the proposed method, we conduct a standard within-distribution comparative

TABLE I
COMPARISON OF SUCCESS RATES (%) ACROSS DIFFERENT SKILLS IN
WITHIN-DISTRIBUTION COMPARATIVE EXPERIMENT

| Method | Pouring | Picking& Placing | Pushing | Slide Opening | Hinge Opening | Average SR |
|----------------------|-------------|------------------|-------------|---------------|---------------|-------------|
| R3M [10] | 64.0 | 64.0 | 52.0 | 60.0 | 60.0 | 60.0 |
| AVDC [17] | 64.0 | 68.0 | 84.0 | 92.0 | 72.0 | 76.0 |
| Track2Act [14] | 88.0 | 80.0 | 76.0 | 80.0 | 88.0 | 82.4 |
| Im2Flow2Act [15] | 84.0 | 92.0 | 88.0 | 92.0 | 84.0 | 88.0 |
| SADiff (Ours) | 92.0 | 96.0 | 92.0 | 96.0 | 88.0 | 92.8 |

experiment, serving as a primary baseline for imitation performance. The scenes and task-related objects are sampled from the exact same distributions as the collected dataset, ensuring a rigorous assessment of the system's ability to recall and execute demonstrated skills.

The experimental results are presented in Table I. SADiff consistently outperforms all baselines across the five skills, achieving a state-of-the-art average success rate of 92.8%. Notably, SADiff surpasses the closest competitor, Im2Flow2Act (88.0%), by a margin of 4.8%. Since Im2Flow2Act also leverages object-centric flow, this performance gain directly highlights the efficacy of explicitly modeling skill-level information, thereby refining the quality of generated motion flows and improving the accuracy of action transformation. Conversely, methods modeling global scene dynamics, including Track2Act (82.4%) and AVDC (76.0%), achieve lower success rates because their full-frame synthesis or dense grid tracking increases susceptibility to background perturbations. SADiff addresses this limitation by centering strictly on task-relevant objects, effectively filtering out visual noise. Moreover, R3M (60.0%) yields the lowest success rate, indicating that pre-trained general-purpose visual representations struggle to disentangle fine-grained, task-specific dynamics from environmental distractors. Collectively, these results confirm that integrating skill-aware priors with focused object dynamics is essential for robust manipulation in within-distribution settings.

3) *Robustness and Generalization Analysis*: To rigorously evaluate the robustness and generalization of SADiff, we design experiments across diverse scenarios that deviate significantly from the training distribution. Specifically, we investigate the performance under four different types of variations involving backgrounds, object instances, object categories, and embodiment. As illustrated in Fig. 5, the four generalization settings are designed as follows:

- *Background Generalization*: This setting introduces variations in lighting conditions and background while keeping the task-related objects consistent with the training set.
- *Intra-Category Instance Generalization*: This setting evaluates the model on unseen instances of task-related objects that differ in color, shape, and physical appearance within the same category.
- *Cross-Category Generalization*: This setting challenges the model by replacing task-related objects with functionally similar objects from entirely different categories (e.g., replacing a cup with a bottle).



Fig. 5. Overview of the generalization evaluation settings. Left: The original collected demonstration. Right: The model is evaluated under four different types of variations involving distribution shifts in backgrounds, intra-category instances, cross-category objects, and embodiment.

- **Cross-Embodiment Generalization:** This setting assesses cross-embodiment generalization by replacing the Franka Panda manipulator with a UR10 robotic arm equipped with a Robotiq two-finger gripper.

The quantitative results averaged across five skills in Fig. 6 demonstrate that SADiff consistently surpasses all baselines across every generalization setting. In the background and intra-category instance generalization scenarios, SADiff achieves robust average success rates of 89.6% and 86.4% by leveraging skill-level guidance to overcome visual variations. This mechanism prevents the incoherent flows observed in Im2Flow2Act and mitigates the visual distractions that degrade the performance of R3M, AVDC, and Track2Act.

In the cross-category generalization setting, SADiff maintains an 82.4% success rate while AVDC and R3M fail completely and other baselines suffer performance drops exceeding 20%. These results indicate that skill priors effectively bridge the gap between different object categories. Furthermore, the cross-embodiment setting reveals that R3M fails due to proprioception mismatches and AVDC cannot synthesize plausible future frames for the unseen robot. While Track2Act and Im2Flow2Act also suffer significant degradation due to limited adaptability, SADiff incurs only a 5.6% performance drop. This stability arises from the skill-specific trajectory priors that enable effective adaptation to novel robotic platforms. Overall, these experiments validate that the skill-aware design of SADiff is essential for robust generalization across visual, object, and embodiment variations.

4) *Instruction-Guided Skill Adaptation Experiment:* To further investigate whether the proposed SADiff can overcome spurious scene-task correlations and prioritize semantic instructions over visual priors, we design a instruction-guided adaptation experiment. In this setup, the physical scene configuration and object placements remain identical to the training distribution, but the language instruction is altered to command a different manipulation skill. As illustrated in Fig. 7, a scene originally associated with a “Picking&Placing” task is redefined as a “Pushing” task during testing. This protocol rigorously evaluates whether the model can flexibly adapt its behavior to new semantic instructions rather than simply memorizing scene-task correlations. We define four specific cross-skill adaptation tasks:

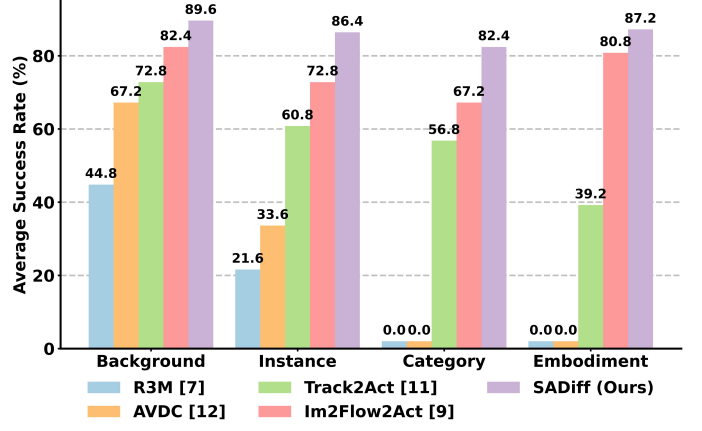


Fig. 6. Average success rate (%) of baselines and SADiff under different generalization scenarios. SADiff consistently achieves the highest average success rate across all four generalization settings.

- Task 1: “Picking&Placing” → “Pushing”
- Task 2: “Pushing” → “Picking&Placing”
- Task 3: “Pouring” → “Picking&Placing”
- Task 4: “Pouring” → “Pushing”

The experimental results in Table II highlight the superior flexibility of SADiff, which achieves an average success rate of 85.0% and significantly outperforms all baselines. R3M and AVDC exhibit a complete inability to adapt with 0% success rates, because they rigidly rely on the specific scene-task correlations learned during training. Similarly, Im2Flow2Act performs poorly with only 16.0% success as its flow generation is overly constrained by the visual scene rather than the language instruction. Although Track2Act fares slightly better with 41.0% due to goal-image conditioning, it still lacks the semantic grasp necessary to consistently execute the new skill. SADiff successfully overcomes these limitations by explicitly classifying the modified instruction into a known skill category during inference. This mechanism allows the model to leverage learned skill representations and generate appropriate actions that align with the new command even when the visual environment suggests a different task.

5) *Ablation Studies:* To systematically assess the individual contributions of each core component, we perform ablation experiments following the identical evaluation protocol

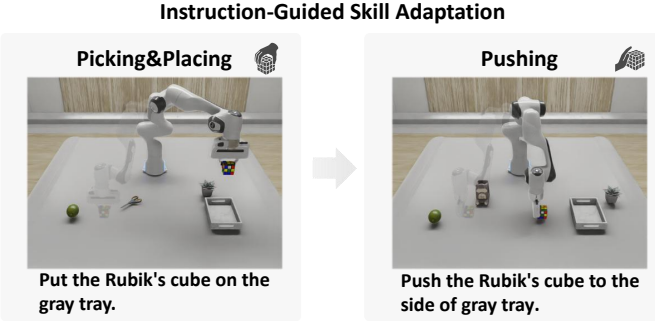


Fig. 7. Examples of the instruction-guided adaptation scenario. The model is evaluated on its ability to switch manipulation skills within an unchanged visual environment solely by following modified language instructions.

TABLE II
COMPARISON OF SUCCESS RATES (%) OF INSTRUCTION-GUIDED SKILL ADAPTATION EXPERIMENT

| Method | Task 1 | Task 2 | Task 3 | Task 4 | Average SR |
|----------------------|-------------|-------------|-------------|-------------|-------------|
| R3M [10] | 0.0 | 0.0 | 0.0 | 0.0 | 0.0 |
| AVDC [17] | 0.0 | 0.0 | 0.0 | 0.0 | 0.0 |
| Track2Act [14] | 44.0 | 52.0 | 32.0 | 36.0 | 41.0 |
| Im2Flow2Act [15] | 20.0 | 16.0 | 12.0 | 16.0 | 16.0 |
| SADiff (Ours) | 88.0 | 84.0 | 88.0 | 80.0 | 85.0 |

utilized for the Robustness and Generalization Analysis in Section V-C3. Specifically, we evaluate performance across background, intra-category instance, and cross-category generalization settings. The three ablated variants are defined as follows:

- *w/o Learnable Skill Tokens (LST)*: This variant removes the learnable skill tokens, along with the related skill classification loss and skill contrastive losses.
- *w/o Skill Contrastive Loss (SCL)*: In this variant, the skill contrastive loss in Eq. (14) is removed.
- *w/o Skill Trajectory Priors (STP)*: In this variant, the skill-specific trajectory prior in Eq. (16) is disabled.

The results are shown in Table III. Removing the Learnable Skill Tokens (LST) causes the average success rate to decline from 86.1% to 75.7%. This drop indicates that without explicit skill representations, the model loses the ability to dynamically modulate multimodal inputs with skill-specific context, severely hampering adaptability in unseen scenarios. Excluding the Skill Contrastive Loss (SCL) results in a decrease to 81.1%, suggesting that without skill-level constraints during the denoising process, the diffusion model generates motion flows that drift from the intended manipulation semantics. Most critically, removing the Skill Trajectory Priors (STP) leads to the sharpest performance degradation to 66.9%. This underscores that trajectory priors are essential for stabilizing the transformation from 2D motion flow to 3D executable actions. Collectively, these findings demonstrate that SADiff relies on the tight coupling of skill-aware encoding, constrained diffusion, and prior-guided transformation to achieve robust generalization.

TABLE III
COMPARISON OF SUCCESS RATES (%) OF ABLATION STUDIES

| Method | Background Generalization | Instance Generalization | Cross-Category Generalization | Average SR |
|---------|---------------------------|-------------------------|-------------------------------|-------------|
| SADiff | 89.6 | 86.4 | 82.4 | 86.1 |
| w/o LST | 84.8 | 74.4 | 68.0 | 75.7 |
| w/o SCL | 86.4 | 81.6 | 75.2 | 81.1 |
| w/o STP | 73.6 | 62.4 | 64.8 | 66.9 |

D. Real-World Experiments

1) *Experiment Setup*: In real-world experiments, we employ a UR5 robotic manipulator equipped with a Robotiq gripper and an Intel RealSense D435i camera, which is mounted on the front-upper side of the workspace to maintain consistency with the simulation setup. To evaluate the generalization ability and zero-shot sim-to-real transfer capability of the proposed SADiff, we directly deploy the model trained purely in simulation without any real-world fine-tuning. We compare our approach against Track2Act [14] and Im2Flow2Act [15], as other baselines like R3M [10] and AVDC [17] lack the capability for direct transfer.

For each skill, we conduct 25 independent rollouts. To rigorously test robustness, we follow the simulation setting by randomly initializing the positions of task-related objects and introducing randomized types and placements for visual distractors in each trial.

2) *Experiment Results*: The results are summarized in Table IV. SADiff achieves an average success rate of 76.0%, outperforming Im2Flow2Act by 21.6% and Track2Act by 25.6% across all five skills. The primary challenge to achieving robust zero-shot sim-to-real transfer lies in pervasive domain discrepancies between simulation and physical environments. These discrepancies include substantial changes in visual scenes and illumination conditions, sensor noise, variations in object types, and embodiment differences. These factors typically cause severe performance degradation for policies trained exclusively in simulation.

Baseline methods struggle considerably under these conditions. Although Track2Act can generate query-point trajectories conditioned on goal images, it is highly sensitive to visual domain shifts, which degrades trajectory quality. Furthermore, its residual policy, which was trained to map 2D trajectories to actions for a specific simulated agent, generalizes poorly to the physical robot. Similarly, Im2Flow2Act leverages Grounding-DINO [62] to identify task-relevant objects, yet it falters when generating object-centric motion flows for novel scenes or unseen instructions. Crucially, its learned policy for converting 2D flow into executable actions relies heavily on fixed camera parameters, limiting its adaptability to real-world setups.

In contrast, SADiff effectively bridges the sim-to-real gap by injecting skill-level knowledge into both the flow generation and action transformation stages. As demonstrated by the real-world results, SADiff retains strong performance without requiring domain randomization or fine-tuning. This consistent superiority validates two key advantages: (1) explicit skill modeling stabilizes diffusion-based motion generation against

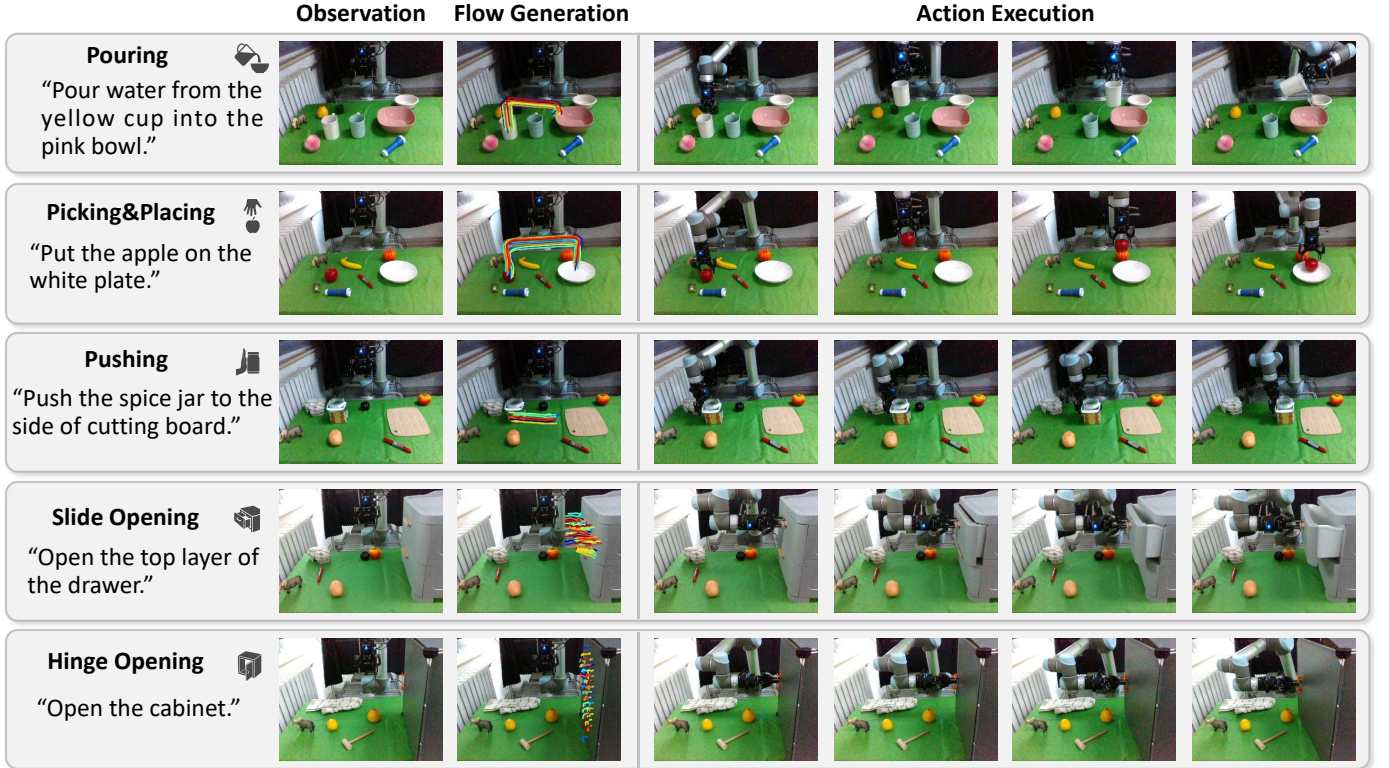


Fig. 8. Visualization of real-world experiments. This figure demonstrates the predicted object-centric motion flow and the corresponding execution trajectories for five manipulation skills in the real world.

TABLE IV
COMPARISON OF SUCCESS RATES (%) ACROSS DIFFERENT SKILLS IN
REAL-WORLD EXPERIMENT

| Method | Pouring | Picking&Placing | Pushing | Slide Opening | Hinge Opening | Average SR |
|----------------------|-------------|-----------------|-------------|---------------|---------------|-------------|
| Track2Act [14] | 44.0 | 52.0 | 56.0 | 48.0 | 52.0 | 50.4 |
| Im2Flow2Act [15] | 56.0 | 60.0 | 56.0 | 58.0 | 42.0 | 54.4 |
| SADiff (Ours) | 72.0 | 80.0 | 80.0 | 76.0 | 72.0 | 76.0 |

visual noise, and (2) the skill-retrieval transformation module reliably converts predicted motion flow into executable actions, even across different robotic embodiments. These findings confirm that SADiff not only excels in simulation but also robustly handles embodiment changes and physical variations in real-world environments. Fig. 8 visualizes the predicted object-centric motion flows and corresponding execution trajectories for five skills, providing further qualitative evidence of the model’s robustness.

In addition, we investigate the time efficiency of the proposed framework in real-world deployment. We measured the average planning time for flow generation, 2D-to-3D mapping, and the average execution time, as shown in Table V. Despite the latency introduced by the utilization of the VLM and the iterative sampling process of the diffusion model, the total time remains within a reasonable range, demonstrating the system’s capability for practical real-time deployment.

3) *Qualitative Analysis under Environmental Variations*: Beyond standard performance metrics, we further qualitatively

TABLE V
PLANNING AND EXECUTION TIME FOR FIVE SKILLS IN REAL-WORLD
EXPERIMENTS

| Time Phases | Pouring | Picking&Placing | Pushing | Slide Opening | Hinge Opening |
|--------------------|---------|-----------------|---------|---------------|---------------|
| Planning Time (s) | 18.4 | 23.1 | 17.2 | 16.9 | 17.8 |
| Execution Time (s) | 28.2 | 21.9 | 10.6 | 14.5 | 15.2 |

evaluate how the policy behaves under extreme visual distractions and domain discrepancies. We extended the experimental evaluation to include real-world scenarios characterized by significant environmental variations. As illustrated in Fig. 9, we introduced three different types of domain shifts to challenge the visual robustness:

- *Different Backgrounds*: We altered the workspace environment by changing tablecloths with varying textures and colors to test robustness against background clutter.
- *Different Lighting*: We introduced complex lighting conditions, including drastic changes in color and intensity, to evaluate the model’s insensitivity to illumination shifts.
- *Different Objects*: We substituted the manipulation targets with unseen object instances that differ in shape, size, and appearance.

We constructed a diverse evaluation set comprising 30 different tasks spanning all five manipulation skills. Despite domain shifts and visual distractions, SADiff demonstrates remarkable adaptability. The qualitative results indicate that

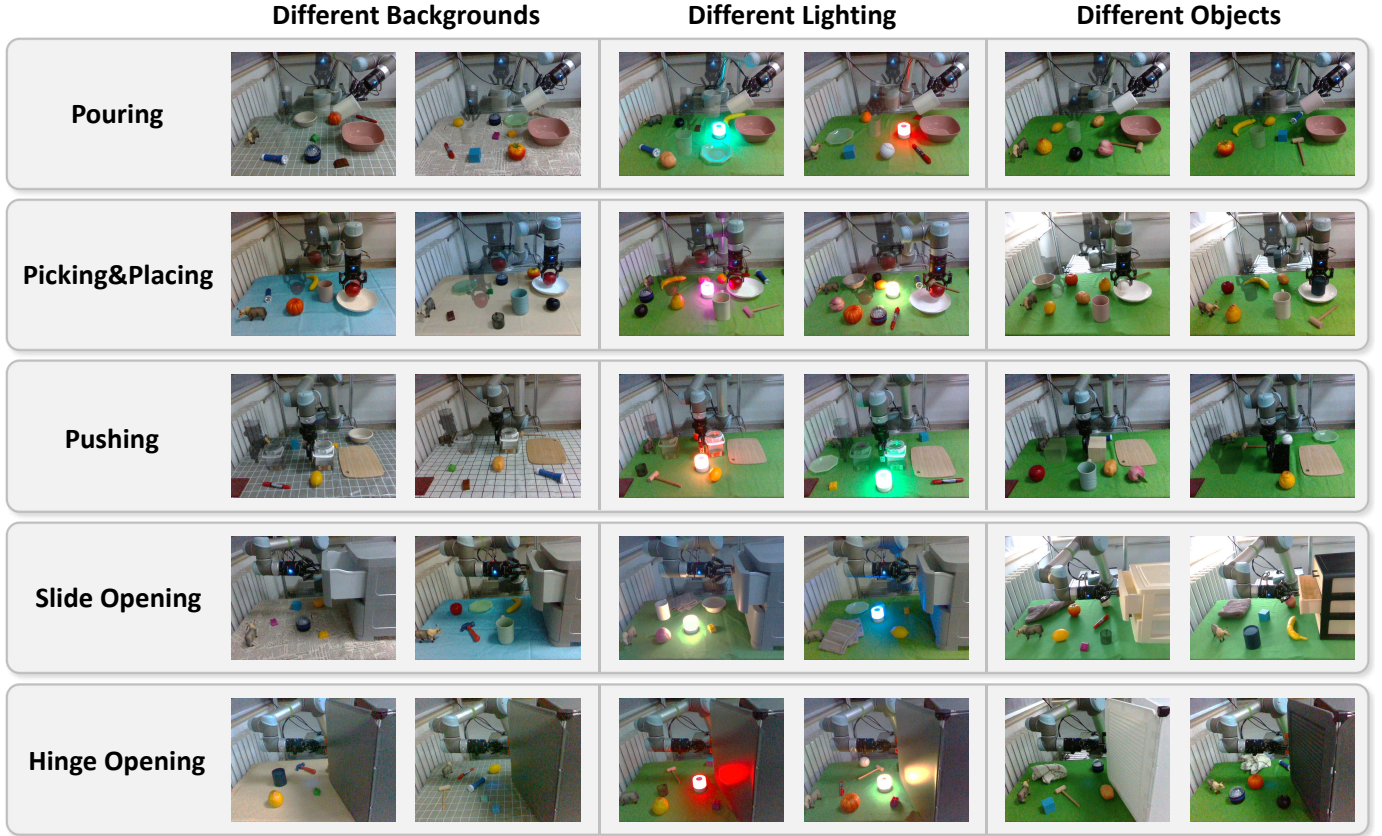


Fig. 9. Qualitative evaluation under environmental variations. We subject the model to a variety of test scenarios featuring diverse backgrounds, complex lighting conditions, and unseen object instances to assess its visual robustness.

our method effectively disentangles target object dynamics from environmental noise. This resilience is attributed to the object-centric nature of the predicted motion flow, which, when combined with the structural constraints of skill-specific priors, enables SADiff to maintain high success rates even in highly unstructured and visually novel environments. These findings further validate the potential of SADiff for robust open-world deployment.

E. Scalability and Composability Experiments

To bridge the gap between specialized manipulation policies and general-purpose robotic agents, it is crucial to verify capabilities beyond standard task repetition. Specifically, real-world deployment requires an agent to not only generalize to new, untrained behaviors but also to seamlessly sequence mastered skills to solve complex, multi-stage problems. To further validate the scalability and robustness of the proposed SADiff in these advanced settings, we consider two essential properties: (1) scalability to unseen skills absent from the training dataset, demonstrating the transferability of our skill representations; and (2) composability for completing long-horizon tasks by chaining multiple skill executions. All experiments utilize the pre-trained SADiff model trained on the proposed IsaacSkill dataset without any additional fine-tuning, evaluated in both simulated and real-world environments.

1) *Scalability to Unseen Skills:* We validate scalability by introducing two unseen skills, “Stacking” and “Wiping”,

which were entirely absent from the training phase. As visualized in Fig. 10, SADiff successfully generates coherent and temporally consistent motion flows for both tasks, enabling reliable translation into stable action trajectories. This zero-shot generalization is achievable because the fundamental skills in our training set (e.g., “Picking & Placing” and “Pushing”) share underlying motion patterns with these novel skills. Consequently, SADiff can effectively approximate the required behaviors for unseen skills like “Stacking” and “Wiping” by leveraging the learned primitives from these foundational skills. These results demonstrate that the proposed SADiff framework can seamlessly extend to semantically and kinematically related behaviors without additional training. Furthermore, this experiment suggests that as the category of fundamental skills in IsaacSkill expands, the model’s capacity to master increasingly complex and diverse tasks will scale correspondingly.

2) *Composability for Long-Horizon Tasks:* To verify the composability of our approach, we evaluate SADiff on long-horizon tasks that require sequential execution of multiple skills. For a complex task instruction such as “Put the apple in the lower drawer”, we leverage Qwen-VL [51] as a VLM-based planner, prompting it to decompose the high-level goal into actionable subtasks conditioned on visual observations and the language command. Subsequently, SADiff generates object-centric motion flows for each subtask and maps them into executable actions. As illustrated in the representative

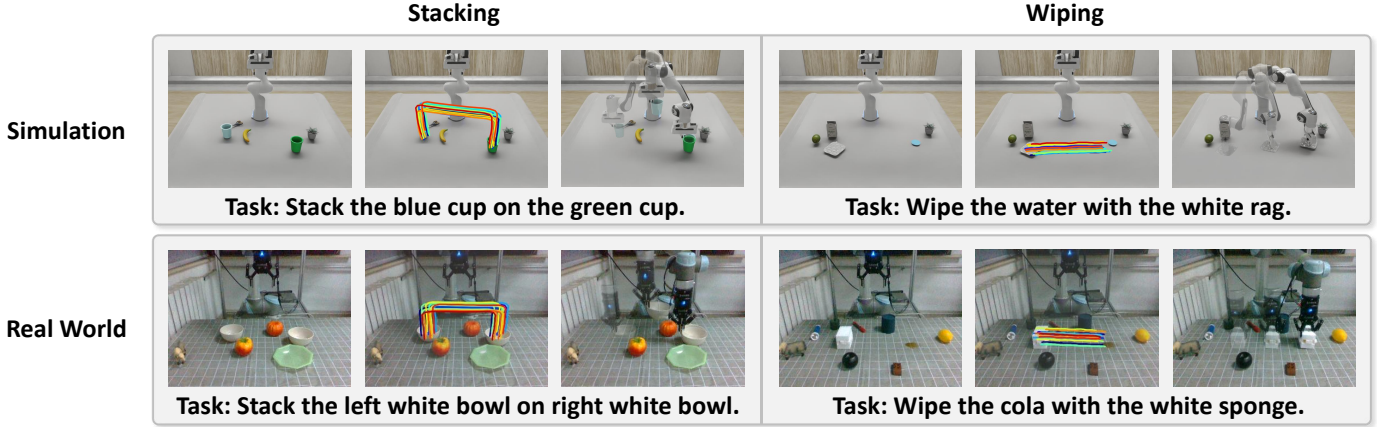


Fig. 10. Demonstration of the scalability of SADiff to unseen skills. We showcase that SADiff can successfully perform new skills (e.g., “Stacking” and “Wiping”) unseen during training in both simulated and real-world environments.

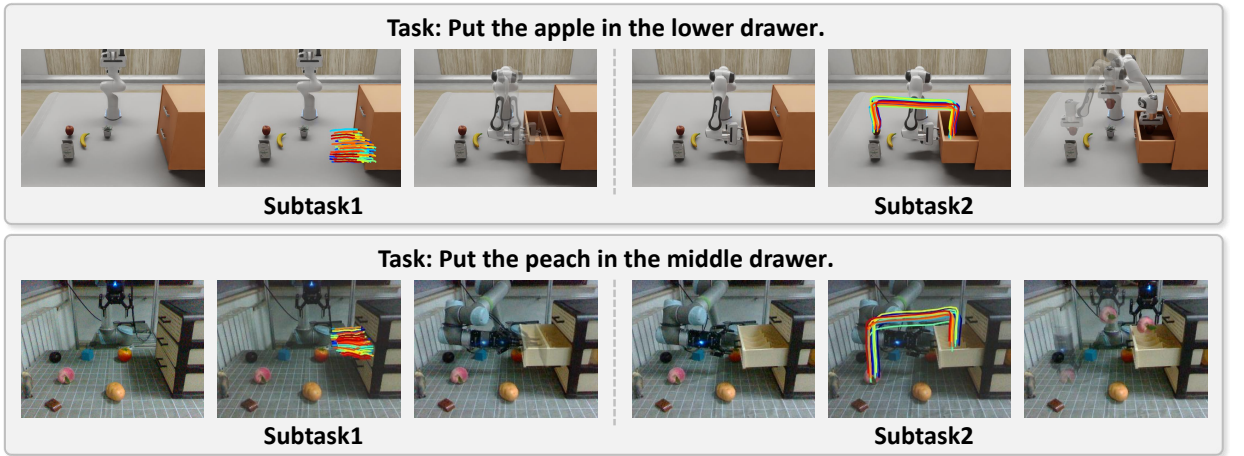


Fig. 11. Demonstration of the composability of SADiff for long-horizon tasks. We assess the model’s capability to execute multi-stage manipulation sequences by decomposing complex instructions into sequential subtasks.

rollouts in Fig. 11, this decoupling strategy enables the flexible composition of diverse skills while leveraging the robust generalization capabilities of SADiff to handle task complexity. The successful execution in both simulation and real-world settings demonstrates the seamless composability of our framework and validates its potential for completing complex, long-horizon manipulation tasks.

VI. CONCLUSION

In this work, we propose SADiff, a skill-aware diffusion framework designed to improve generalization in robotic manipulation through explicit modeling of skill-level information. By integrating a skill-aware encoding module equipped with learnable skill tokens, a skill-constrained diffusion model, and a skill-retrieval transformation strategy, SADiff effectively captures shared skill-level information within the same skill domain and systematically integrates it across the encoding, generation, and execution phases. This allows it to precisely generate object-centric motion flow and robustly map the 2D flow to executable 3D actions in diverse scenarios and environments. Furthermore, we construct a high-fidelity IsaacSkill dataset, which not only enables a comprehensive assessment of

specific skill capabilities but also provides the realistic dynamics required to support robust sim-to-real transfer. Extensive experiments in both simulation and real-world settings demonstrate that SADiff significantly outperforms existing methods in generalization to unseen objects, varying environments, and distinct embodiments, and achieves zero-shot sim-to-real transfer. These results underscore the pivotal role of explicitly modeling skill-level knowledge and integrating it throughout all phases of the pipeline. Moreover, SADiff demonstrates scalability and composability by successfully generalizing to unseen skills and composing multiple learned skills to execute long-horizon manipulation tasks.

Although SADiff demonstrates strong generalization and zero-shot sim-to-real transfer, it still faces several limitations. Firstly, the skill taxonomy is manually specified, which constrains the expressiveness of the skill space when extending the framework to more complex or fine-grained manipulation tasks. Future work could explore unsupervised skill discovery, such as using VQ-VAE [63] to extract and structure semantic skills from various demonstrations. Secondly, the 2D motion flow representation struggles to fully resolve spatial dynamics in tasks with out-of-plane rotations (e.g., unscrewing a bottle

cap). Future work could extend our framework to utilize 3D motion flow [64] for more precise robotic manipulation.

REFERENCES

- [1] H. Zhou, X. Yao, Y. Meng, S. Sun, Z. Bing, K. Huang, and A. Knoll, “Language-conditioned learning for robotic manipulation: A survey,” *arXiv preprint arXiv:2312.10807*, 2023.
- [2] W. Zhao, J. Chen, Z. Meng, D. Mao, R. Song, and W. Zhang, “Vlmpc: Vision-language model predictive control for robotic manipulation,” in *Robotics: Science and Systems*, 2024.
- [3] O. Mees, L. Hermann, and W. Burgard, “What matters in language conditioned robotic imitation learning over unstructured data,” *IEEE Robotics and Automation Letters*, vol. 7, no. 4, pp. 11 205–11 212, 2022.
- [4] T. Ma, J. Zhou, Z. Wang, R. Qiu, and J. Liang, “Contrastive imitation learning for language-guided multi-task robotic manipulation,” in *Conference on Robot Learning*. PMLR, 2025, pp. 4651–4669.
- [5] F. Lin, Y. Hu, P. Sheng, C. Wen, J. You, and Y. Gao, “Data scaling laws in imitation learning for robotic manipulation,” in *The Thirteenth International Conference on Learning Representations*.
- [6] Z. Chen, Z. Mandi, H. Bharadhwaj, M. Sharma, S. Song, A. Gupta, and V. Kumar, “Semantically controllable augmentations for generalizable robot learning,” *The International Journal of Robotics Research*, vol. 44, no. 10-11, pp. 1705–1726, 2025.
- [7] T. Zhang, Z. McCarthy, O. Jow, D. Lee, X. Chen, K. Goldberg, and P. Abbeel, “Deep imitation learning for complex manipulation tasks from virtual reality teleoperation,” in *2018 IEEE international conference on robotics and automation (ICRA)*. Ieee, 2018, pp. 5628–5635.
- [8] T. Z. Zhao, V. Kumar, S. Levine, and C. Finn, “Learning fine-grained bimanual manipulation with low-cost hardware,” *arXiv preprint arXiv:2304.13705*, 2023.
- [9] Y. J. Ma, S. Sodhani, D. Jayaraman, O. Bastani, V. Kumar, and A. Zhang, “Vip: Towards universal visual reward and representation via value-implicit pre-training,” in *The Eleventh International Conference on Learning Representations*.
- [10] S. Nair, A. Rajeswaran, V. Kumar, C. Finn, and A. Gupta, “R3m: A universal visual representation for robot manipulation,” in *Conference on Robot Learning*. PMLR, 2023, pp. 892–909.
- [11] J. Zeng, Q. Bu, B. Wang, W. Xia, L. Chen, H. Dong, H. Song, D. Wang, D. Hu, P. Luo *et al.*, “Learning manipulation by predicting interaction,” in *Robotics: Science and Systems*, 2024.
- [12] H. Bharadhwaj, D. Dwibedi, A. Gupta, S. Tulsiani, C. Doersch, T. Xiao, D. Shah, F. Xia, D. Sadigh, and S. Kirmani, “Gen2act: Human video generation in novel scenarios enables generalizable robot manipulation,” *arXiv preprint arXiv:2409.16283*, 2024.
- [13] F. Ni, J. Hao, S. Wu, L. Kou, J. Liu, Y. Zheng, B. Wang, and Y. Zhuang, “Generate subgoal images before act: Unlocking the chain-of-thought reasoning in diffusion model for robot manipulation with multimodal prompts,” in *Proceedings of the IEEE/CVF Conference on Computer Vision and Pattern Recognition*, 2024, pp. 13 991–14 000.
- [14] H. Bharadhwaj, R. Mottaghi, A. Gupta, and S. Tulsiani, “Track2act: Predicting point tracks from internet videos enables generalizable robot manipulation,” in *European Conference on Computer Vision*. Springer, 2024, pp. 306–324.
- [15] M. Xu, Z. Xu, Y. Xu, C. Chi, G. Wetzstein, M. Veloso, and S. Song, “Flow as the cross-domain manipulation interface,” in *8th Annual Conference on Robot Learning*, 2024.
- [16] Y. Chen, P. Li, Y. Huang, J. Yang, K. Chen, and L. Wang, “Ec-flow: Enabling versatile robotic manipulation from action-unlabeled videos via embodiment-centric flow,” *arXiv preprint arXiv:2507.06224*, 2025.
- [17] P. C. Ko, J. Mao, Y. Du *et al.*, “Learning to act from actionless videos through dense correspondences,” in *Proceedings of the Twelfth International Conference on Learning Representations*, 2023.
- [18] K. Fang, Y. Zhu, S. Savarese, and L. Fei-Fei, “Discovering generalizable skills via automated generation of diverse tasks,” *arXiv preprint arXiv:2106.13935*, 2021.
- [19] Z. Liang, Y. Mu, H. Ma, M. Tomizuka, M. Ding, and P. Luo, “Skilldiffuser: Interpretable hierarchical planning via skill abstractions in diffusion-based task execution,” in *Proceedings of the IEEE/CVF Conference on Computer Vision and Pattern Recognition*, 2024, pp. 16 467–16 476.
- [20] Y. Yao, S. Liu, H. Song, D. Qu, Q. Chen, Y. Ding, B. Zhao, Z. Wang, X. Li, and D. Wang, “Think small, act big: Primitive prompt learning for lifelong robot manipulation,” in *Proceedings of the Computer Vision and Pattern Recognition Conference*, 2025, pp. 22 573–22 583.
- [21] T. Yu, D. Quillen, Z. He, R. Julian, K. Hausman, C. Finn, and S. Levine, “Meta-world: A benchmark and evaluation for multi-task and meta reinforcement learning,” in *Conference on robot learning*. PMLR, 2020, pp. 1094–1100.
- [22] S. James, Z. Ma, D. R. Arrojo, and A. J. Davison, “Rlbench: The robot learning benchmark & learning environment,” *IEEE Robotics and Automation Letters*, vol. 5, no. 2, pp. 3019–3026, 2020.
- [23] B. Liu, Y. Zhu, C. Gao, Y. Feng, Q. Liu, Y. Zhu, and P. Stone, “Libero: Benchmarking knowledge transfer for lifelong robot learning,” *Advances in Neural Information Processing Systems*, vol. 36, pp. 44 776–44 791, 2023.
- [24] M. Mittal, P. Roth, J. Tigue, A. Richard, O. Zhang, P. Du, A. Serrano-Muñoz, X. Yao, R. Zurbrügg, N. Rudin *et al.*, “Isaac lab: A gpu-accelerated simulation framework for multi-modal robot learning,” *arXiv preprint arXiv:2511.04831*, 2025.
- [25] O. Kroemer, S. Niekum, and G. Konidaris, “A review of robot learning for manipulation: Challenges, representations, and algorithms,” *Journal of machine learning research*, vol. 22, no. 30, pp. 1–82, 2021.
- [26] M. Drolet, S. Stepputis, S. Kailas, A. Jain, J. Peters, S. Schaal, and H. B. Amor, “A comparison of imitation learning algorithms for bimanual manipulation,” *IEEE Robotics and Automation Letters*, 2024.
- [27] Z. Li, A. Chapin, E. Xiang, R. Yang, B. Machado, N. Lei, E. Dellandrea, D. Huang, and L. Chen, “Robotic manipulation via imitation learning: Taxonomy, evolution, benchmark, and challenges,” *arXiv preprint arXiv:2508.17449*, 2025.
- [28] A. Mandlekar, D. Xu, J. Wong, S. Nasiriany, C. Wang, R. Kulkarni, L. Fei-Fei, S. Savarese, Y. Zhu, and R. Martín-Martín, “What matters in learning from offline human demonstrations for robot manipulation,” *arXiv preprint arXiv:2108.03298*, 2021.
- [29] C. Chi, Z. Xu, S. Feng, E. Cousineau, Y. Du, B. Burchfiel, R. Tedrake, and S. Song, “Diffusion policy: Visuomotor policy learning via action diffusion,” *The International Journal of Robotics Research*, p. 02783649241273668, 2023.
- [30] S. Stepputis, J. Campbell, M. Philipp, S. Lee, C. Baral, and H. Ben Amor, “Language-conditioned imitation learning for robot manipulation tasks,” *Advances in Neural Information Processing Systems*, vol. 33, pp. 13 139–13 150, 2020.
- [31] X. Yao, T. Blei, Y. Meng, Y. Zhang, H. Zhou, Z. Bing, K. Huang, F. Sun, and A. Knoll, “Long-horizon language-conditioned imitation learning for robotic manipulation,” *IEEE/ASME Transactions on Mechatronics*, 2025.
- [32] M. Shridhar, L. Manuelli, and D. Fox, “Cliport: What and where pathways for robotic manipulation,” in *Conference on robot learning*. PMLR, 2022, pp. 894–906.
- [33] A. Radford, J. W. Kim, C. Hallacy, A. Ramesh, G. Goh, S. Agarwal, G. Sastry, A. Askell, P. Mishkin, J. Clark *et al.*, “Learning transferable visual models from natural language supervision,” in *International conference on machine learning*. PMLR, 2021, pp. 8748–8763.
- [34] M. Shridhar, L. Manuelli, and D. Fox, “Perceiver-actor: A multi-task transformer for robotic manipulation,” in *Conference on Robot Learning*. PMLR, 2023, pp. 785–799.
- [35] A. Jaegle, S. Borgeaud, J.-B. Alayrac, C. Doersch, C. Ionescu, D. Ding, S. Koppula, D. Zoran, A. Brock, E. Shelhamer *et al.*, “Perceiver io: A general architecture for structured inputs & outputs,” *arXiv preprint arXiv:2107.14795*, 2021.
- [36] K. Grauman, A. Westbury, E. Byrne, Z. Chavis, A. Furnari, R. Girdhar, J. Hamburger, H. Jiang, M. Liu, X. Liu *et al.*, “Ego4d: Around the world in 3,000 hours of egocentric video,” in *Proceedings of the IEEE/CVF conference on computer vision and pattern recognition*, 2022, pp. 18 995–19 012.
- [37] A. O’Neill, A. Rehman, A. Maddukuri, A. Gupta, A. Padalkar, A. Lee, A. Pooley, A. Gupta, A. Mandlekar, A. Jain *et al.*, “Open x-embodiment: Robotic learning datasets and rt-x models: Open x-embodiment collaboration 0,” in *2024 IEEE International Conference on Robotics and Automation (ICRA)*. IEEE, 2024, pp. 6892–6903.
- [38] T. Xiao, I. Radosavovic, T. Darrell, and J. Malik, “Masked visual pre-training for motor control,” *arXiv preprint arXiv:2203.06173*, 2022.
- [39] C. Wen, X. Lin, J. So, K. Chen, Q. Dou, Y. Gao, and P. Abbeel, “Any-point trajectory modeling for policy learning,” *arXiv preprint arXiv:2401.00025*, 2023.
- [40] R. P. Wolf, Y. Shi, S. Liu, and R. Rayyes, “Diffusion models for robotic manipulation: A survey,” *Frontiers in Robotics and AI*, vol. 12, p. 1606247, 2025.
- [41] K. Zhang, P. Yun, J. Cen, J. Cai, D. Zhu, H. Yuan, C. Zhao, T. Feng, M. Y. Wang, Q. Chen *et al.*, “Generative artificial intelligence in robotic manipulation: A survey,” *arXiv preprint arXiv:2503.03464*, 2025.

[42] X. Ma, S. Patidar, I. Haughton, and S. James, “Hierarchical diffusion policy for kinematics-aware multi-task robotic manipulation,” in *Proceedings of the IEEE/CVF Conference on Computer Vision and Pattern Recognition*, 2024, pp. 18 081–18 090.

[43] T. Pearce, T. Rashid, A. Kanervisto, D. Bignell, M. Sun, R. Georgescu, S. V. Macua, S. Z. Tan, I. Momennejad, K. Hofmann *et al.*, “Imitating human behaviour with diffusion models,” *arXiv preprint arXiv:2301.10677*, 2023.

[44] M. Reuss, M. Li, X. Jia, and R. Lioutikov, “Goal conditioned imitation learning using score-based diffusion policies,” in *Robotics: Science and Systems*, 2023.

[45] Y. Ze, G. Zhang, K. Zhang, C. Hu, M. Wang, and H. Xu, “3d diffusion policy: Generalizable visuomotor policy learning via simple 3d representations,” in *Proceedings of Robotics: Science and Systems (RSS)*, 2024.

[46] H. Xue, J. Ren, W. Chen, G. Zhang, Y. Fang, G. Gu, H. Xu, and C. Lu, “Reactive diffusion policy: Slow-fast visual-tactile policy learning for contact-rich manipulation,” in *Proceedings of Robotics: Science and Systems (RSS)*, 2025.

[47] T. Chen, Y. Mu, Z. Liang, Z. Chen, S. Peng, Q. Chen, M. Xu, R. Hu, H. Zhang, X. Li *et al.*, “G3flow: Generative 3d semantic flow for pose-aware and generalizable object manipulation,” in *Proceedings of the Computer Vision and Pattern Recognition Conference*, 2025, pp. 1735–1744.

[48] H. Zhen, Q. Sun, H. Zhang, J. Li, S. Zhou, Y. Du, and C. Gan, “Tesseract: learning 4d embodied world models,” *arXiv preprint arXiv:2504.20995*, 2025.

[49] Y. Du, S. Yang, B. Dai, H. Dai, O. Nachum, J. Tenenbaum, D. Schuurmans, and P. Abbeel, “Learning universal policies via text-guided video generation,” *Advances in neural information processing systems*, vol. 36, pp. 9156–9172, 2023.

[50] C. Wen, X. Lin, J. So, K. Chen, Q. Dou, Y. Gao, and P. Abbeel, “Any-point trajectory modeling for policy learning,” *Robotics Science and Systems 2024*, 2024.

[51] J. Bai, S. Bai, S. Yang, S. Wang, S. Tan, P. Wang, J. Lin, C. Zhou, and J. Zhou, “Qwen-vl: A versatile vision-language model for understanding, localization, text reading, and beyond,” *arXiv preprint arXiv:2308.12966*, 2023.

[52] C. Doersch, Y. Yang, M. Vecerik *et al.*, “Tapir: Tracking any point with per-frame initialization and temporal refinement,” in *Proceedings of the IEEE/CVF International Conference on Computer Vision*, 2023, pp. 10 061–10 072.

[53] Z. Wang and J.-C. Liu, “Translating math formula images to latex sequences using deep neural networks with sequence-level training,” *International Journal on Document Analysis and Recognition (IJDAR)*, vol. 24, no. 1, pp. 63–75, 2021.

[54] A. Vaswani, “Attention is all you need,” *Advances in Neural Information Processing Systems*, 2017.

[55] D. P. Kingma, M. Welling *et al.*, “An introduction to variational autoencoders,” *Foundations and Trends® in Machine Learning*, vol. 12, no. 4, pp. 307–392, 2019.

[56] Y. Guo, C. Yang, A. Rao, Z. Liang, Y. Wang, Y. Qiao, M. Agrawala, D. Lin, and B. Dai, “Animatediff: Animate your personalized text-to-image diffusion models without specific tuning,” *arXiv preprint arXiv:2307.04725*, 2023.

[57] R. Rombach, A. Blattmann, D. Lorenz, P. Esser, and B. Ommer, “High-resolution image synthesis with latent diffusion models,” in *Proceedings of the IEEE/CVF conference on computer vision and pattern recognition*, 2022, pp. 10 684–10 695.

[58] J. J. Moré, “The levenberg-marquardt algorithm: implementation and theory,” in *Numerical analysis: proceedings of the biennial Conference held at Dundee, June 28–July 1, 1977*. Springer, 2006, pp. 105–116.

[59] L. Yang, B. Kang, Z. Huang, Z. Zhao, X. Xu, J. Feng, and H. Zhao, “Depth anything v2,” *Advances in Neural Information Processing Systems*, vol. 37, pp. 21 875–21 911, 2024.

[60] R. Rombach, A. Blattmann, D. Lorenz, P. Esser, and B. Ommer, “High-resolution image synthesis with latent diffusion models,” in *Proceedings of the IEEE/CVF conference on computer vision and pattern recognition*, 2022, pp. 10 684–10 695.

[61] E. J. Hu, Y. Shen, P. Wallis, Z. Allen-Zhu, Y. Li, S. Wang, L. Wang, and W. Chen, “LoRA: Low-rank adaptation of large language models,” in *International Conference on Learning Representations*, 2022.

[62] S. Liu, Z. Zeng, T. Ren, F. Li, H. Zhang, J. Yang, Q. Jiang, C. Li, J. Yang, H. Su *et al.*, “Grounding dino: Marrying dino with grounded pre-training for open-set object detection,” in *European conference on computer vision*. Springer, 2024, pp. 38–55.

[63] A. Van Den Oord, O. Vinyals *et al.*, “Neural discrete representation learning,” *Advances in neural information processing systems*, vol. 30, 2017.

[64] C. Yuan, C. Wen, T. Zhang, and Y. Gao, “General flow as foundation affordance for scalable robot learning,” *arXiv preprint arXiv:2401.11439*, 2024.